**PAPER • OPEN ACCESS**

# Modelling of major phases formation during solidification of Ferro-Silicon-Magnesium

To cite this article: S Gouttebroze *et al* 2023 *IOP Conf. Ser.: Mater. Sci. Eng.* **1281** 012052

View the article online for updates and enhancements.

## You may also like

# Modelling of major phases formation during solidification of Ferro-Silicon-Magnesium

**S Gouttebroze[1], A Marthinsen[1], B Kroka[2], A Götz[2], E Ott[2]**

[1] SINTEF Industry, Forskningsveien 1, 0373 Oslo, Norway
[2] Elkem Silicon Product Development, Fiskåveien 100, 4621 Kristiansand S, Norway


sylvain.gouttebroze@sintef.no

**Abstract**. Ductile cast iron, also known as nodular cast iron, is a graphite-rich cast iron with high impact and fatigue resistance, due to its nodular graphite inclusions. Ductile cast iron is produced by incorporating additives (often FeSi alloys) to the iron base metal at different production steps to obtain the desired graphite shape. A crucial step is the addition of Magnesium to promote the spheroidization of the graphite. The most common method is by adding crushed and sized Ferro-Silicon-Magnesium (FSM). The alloy composition, microstructure, and sizing are assumed to affect the key parameters of this reaction, namely, reactivity, recovery, and slag formation. Therefore, the study of the solidification of FSM is important to understand and predict its performance at the foundries. The present work aims at understanding and predicting numerically the formation of the major phases during the solidification process. Two approaches have been used: thermodynamic calculations through Thermo-Calc solver and phase field modelling using MICRESS. The models have been calibrated by comparison with advanced statistical characterization of the microstructure. The results indicate a competitive growth of the major phases and transformation of phases in solid state that can be emulated by the model.

## 1. Introduction

Ferrosilicon magnesium (FSM) alloys are widely used in cast iron industry as an additive in production of ductile cast iron to promote the formation of spheroidal graphite nodules. The presence of spheroidal graphite results in a material with both good ductility and high strength. [1]

Though FSM alloys are used abundantly in the production of ductile cast iron and their composition is assumed to impact important parameters of the melt treatment (such as reactivity, recovery and slag formation), there is scarce knowledge about how variation in the composition, microstructure and subsequent sizing of the FSM alloys affect their performance in the ductile iron casting process. To bridge this knowledge gap, it is important to understand the solidification process of the FSM alloys in order to tailor their microstructure and resulting properties.

FSM alloys cover a wide range of compositions, the main elements being Fe, Si and Mg. The amount of Si typically varies between 40-50 wt%, whereas Mg is in the range 5-10 wt%. In addition, the FSM alloys often contain small amounts of additional elements, such as Ca, Al, Ti, and Rare Earth Elements (like La and Ce). This large compositional space implies that different phases are present for different alloys, in different amounts and with different morphologies. Processing conditions (in particular cooling rate) can also affect the microstructure. The main phases, which are present in nearly every FSM alloy, include $FeSi$, $FeSi_2$, $Mg_2Si$ and pure Si. The $FeSi_2$ phase has a high

temperature form (α-FeSi$_2$) which has tetragonal crystal structure and a low temperature form (β-FeSi$_2$) which has an orthorhombic crystal structure. The high temperature α-FeSi$_2$, is also rich in Fe vacancies, making the stoichiometry closer to FeSi$_{2.33}$, and later denoted as Fe$_3$Si$_7$.

In this work, two different modelling approaches have been used to predict and understand the formation of the main phases in FSM alloys. A python-based thermodynamic solidification model was developed to predict the solidification path and resulting phase fractions by relying on Thermo-Calc software [2], and a phase field software, Micress [3], was used to build a more comprehensive understanding about the solidification process and the effects of phases morphology. Two different FSM alloys have been considered and the model predictions compared with experimental data.

## 2. Methodology

### 2.1. Experimental work and microstructure characterization

The FSM alloys were produced at the Elkem Pilot Station using the Casting Simulator setup. A charge mix of 50 kg consisting of ferrosilicon with some alloying elements was molten in a 250 kW induction furnace. The melt was cast via a graphite runner onto a traversing water-cooled copper plate which was divided into three sections allowing to cast variable thicknesses in a single operation. Target casting thicknesses were 15 and 30 mm. Vertical samples were taken through the cast layer thickness while avoiding non-representative areas with oxides or slag inclusions (see Figure 1).



Figure 1. As-cast FSM material (left) and sample embedded in epoxy for SEM characterization (right)

The analysis of the material focused mostly on chemical composition and microstructure. The chemical composition what obtained by XRF analysis. The microstructure characterization was performed using the Advanced Mineral Identification and Characterization System (AMICS) [4], which is a new method that merges scanning electron microscopy (SEM), imaging with X-ray spectroscopy (EDS), and phase identification. It allows automated and very fast mapping of phases covering large areas (up to 30 mm$^2$ in this study). The core feature of AMICS is the use of image analysis of the backscatter electron images (BSE) to segment regions of the microstructure to limit the number of necessary X-ray measurements to map the individual phase areas. This is combined with fast search/match through a database of X-ray spectra specific to each material. This database of X-ray spectra has been constructed using samples from both the production plants and the pilot casting simulator to cover a larger range of cooling rate and chemical composition. AMICS provides (x, y) coordinates of electron signals, EDS spectra and phase ID's and merges these into regions where size and neighborhoods are quantified.

Using AMICS, FSM microstructures are evaluated and quantified on plane sections through the entire cast thickness with a spatial resolution down to 1μm. Very small grains could be missed or considered part of another phase but the accuracy for the large phases is very good. In addition, the operator needs to carefully evaluate possible overlap in BSE contrast between phases and adjust accordingly the segmentation parameters. AMICS overviews are also used to locate interesting features or phases configurations for detailed EDS analysis of phase compositions down to trace elements level. The resulting data are used to provide input for microstructure model calibration and to correlate process data with microstructure evolution.

## 2.2. Thermodynamic modelling

Thermodynamic simulations were performed using the Calphad Software Thermo-Calc [2]. An in-house database was used in the simulations, as none of the commercial databases available at SINTEF could properly handle solidification of the FSM alloys, given the very different Fe and Si compositions compared with steel (focus of TCFE commercial database). The in-house database was built from thermodynamic literature data. It includes all the binary systems, and also some ternary systems assessments: Fe-Si-Ca, Fe-Si-Mg, Fe-Si-Al, Mg-Si-Al, Mg-Si-Ca. A python-based modelling framework was built and coupled to Thermo-Calc through the python module TCPython, to facilitate high-throughput calculations, storage, and analysis of output data. As part of the modelling framework, a solidification model was developed to extend the capabilities by including solid-solid reactions, and accounting for the thermal history of the solidified microstructure.

The solid-solid reactions module implemented in the python modelling framework takes as input the temperature history of the solidified microstructure, i.e., a list of times and temperatures as well as an initial state of the system including phases fraction and compositions. For each temperature step, the model runs an equilibrium calculation through the Thermo-Calc solver for the composition of the liquid part of the system as in a Scheil calculation. If no solid-solid phase transformation is activated, the resulting solidification path is exactly equal to the Scheil calculation integrated in Thermo-Calc. Otherwise, between time step $t$ and $t+dt$, the user-defined solid-solid reactions are computed, and the solid domain is updated.

The kinetics of solid-solid phase transformations are modelled using the Johnson-Mehl-Avrami-Kolmogorov (JMAK) equation, where the ratio between the fraction of a given phase $\theta$ at time $t$ and the equilibrium phase fraction at a given temperature $T$ is given by:

$$\frac{f_\theta(t)}{f_\theta(eq)} = 1 - \exp\left(-K(T)t^n\right) \text{ , with } K(T) = K_0 \exp(-\frac{Q_r}{RT}) \tag{1}$$

where $K$ is the reaction rate constant, $K_0$ is the frequency factor, $Q_r$ is the activation energy, and $n$ is the Avrami exponent, where $n=4$ under the assumption of nucleation and growth in three dimensions. The cooling curve is discretized in iso-thermal steps and the additivity ule is applied.

## 2.3. Phase field modelling

To study the effect of phase morphology on the formation of the two major phases in FSM, FeSi and $Fe_3Si_7$, and to get a more comprehensive picture of the solidification process, a phase field model was developed using the software MICRESS [3]. FeSi and $Fe_3Si_7$ formation determines the main features of the solidified microstructure as they are often the first to nucleate and represent a large volume fraction (>80%). In contrast to thermodynamic simulations, phase field models allow to study the effect of local phenomena on the solidification process, including local composition gradients, elemental diffusion, and nucleation and growth of phases.

The phase field model in Micress was coupled to the same thermodynamic database used for the thermodynamic simulations with Thermo-Calc. A significant number of input parameters were needed for the phase-field model to describe the different phases and their interactions with neighboring phases and the liquid phase. Extensive parameter testing was therefore done to optimize the set of parameters to fit experimental observations of the FSM morphology. The simulation domains were limited to 2D rectangular domains due to the much higher computational cost of running 3D simulations, with typical size in the range of 200-300 μm and grid size of 1-2 μm.

## 3. Results

### 3.1. Experimental measurements and observations

In this study, two FSM alloys were considered and compared. Their compositions mainly differ in the Fe/Si concentration, where Alloy 2 is richer in Si than Alloy 1. The concentrations of the main elements in the two alloys (Fe, Si and Mg) are listed in Table 1.

Table 1: Concentration in wt% of main elements (Fe, Si, Mg) in Alloy 1 and Alloy 2

| Alloy name | Fe | Si | Mg | Other |
|---|---|---|---|---|
| Alloy 1 (LowSi) | 47.91 | 43.49 | 5.81 | 2.79 |
| Alloy 2 (HighSi) | 44.57 | 47.16 | 5.45 | 2.82 |

The cross-sections through the thickness of the samples were analyzed with AMICS. The phases spatial distribution for Alloy 1 and Alloy 2 are shown in Figure 2 at three locations: one from the top of the cross section, one from the middle and one from the bottom, close to the copper plate on which the alloys were cast. The bottom of the cast has solidified at a higher cooling rate than the middle and top segments, which results in a finer grain structure. The composition change yields a visually significant variation in the phase fractions and morphology. The lower Si content of Alloy 1 results in a larger fraction of FeSi (yellow) compared to $FeSi_2$ (green) as expected from the liquidus projection in Figure 3 that shows to increasing proximity of the boundary to $Fe_3Si_7$ domain. The variation between alloys is much larger than through the thickness of the samples. This indicates that this material does not undergo significant macrosegregation at these cooling rates.

Furthermore, the morphology of the FeSi phase, usually dendritic, is somewhat more globular in Alloy 1 than in Alloy 2. The $FeSi_2$ phase on the other hand, forms elongated rod-like grains. In both alloys, the FeSi phase is largely encapsulated by the FeSi2 phase. In some areas, the FeSi phase is seen in the middle of the bulk of $FeSi_2$, whereas in other areas, only a thin layer of $FeSi_2$ encapsules the FeSi. Only the low temperature form of $FeSi_2$ is observed.
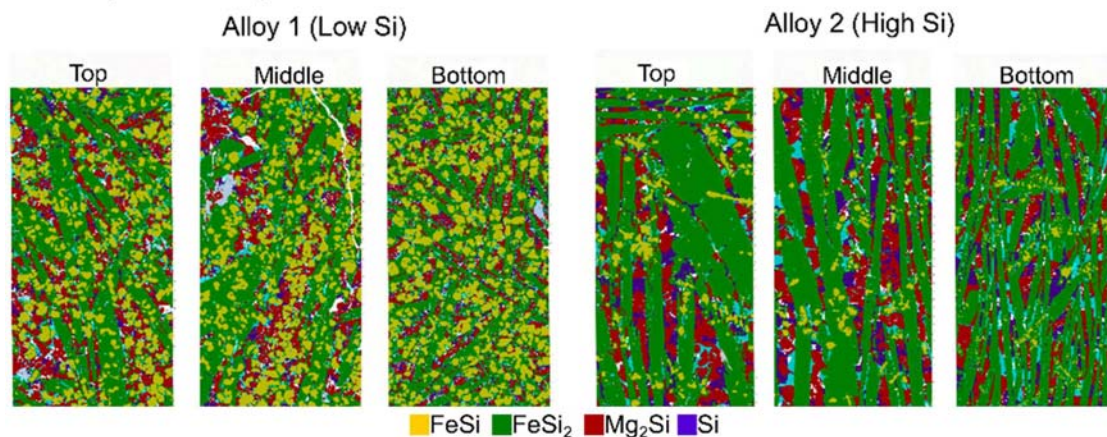


*Figure 2 Experimental phases maps generated by AMICS of Alloy 1 (left) and Alloy 2 (right). The domain width is approximately 800 µm.*

These features are even clearer in the zoomed images presented in Figure 4. FeSi could form large dendrites (left image) that will disturb the growth of $FeSi_2$ phase. In the central image, all the small remaining FeSi areas are coated with $FeSi_2$, present as large bulky rods and smaller excrescence near FeSi. On the right picture, the $FeSi_2$ rods are growing independently following the complex temperature gradient present at the surface (the radiation cooling combined with the possible presence of oxide layer could leads to non-uniform, high cooling rates).
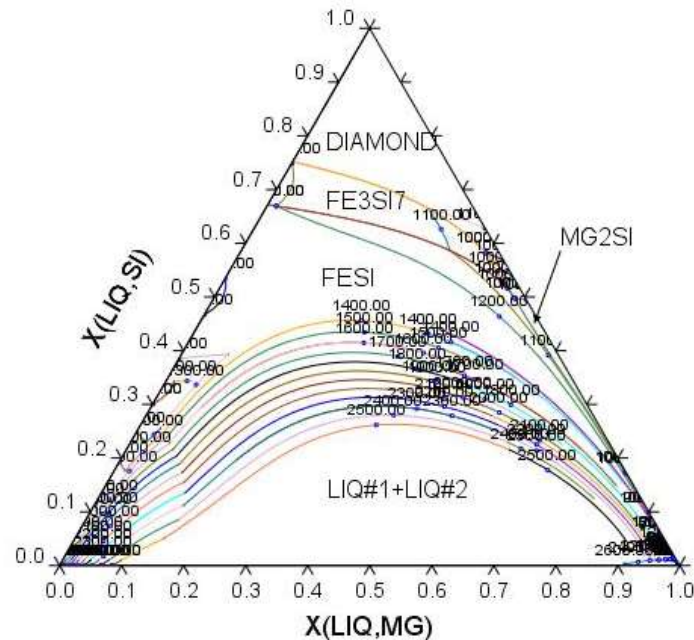
*Figure 3. Liquidus projection computed from SINTEF database using Thermo-Calc*
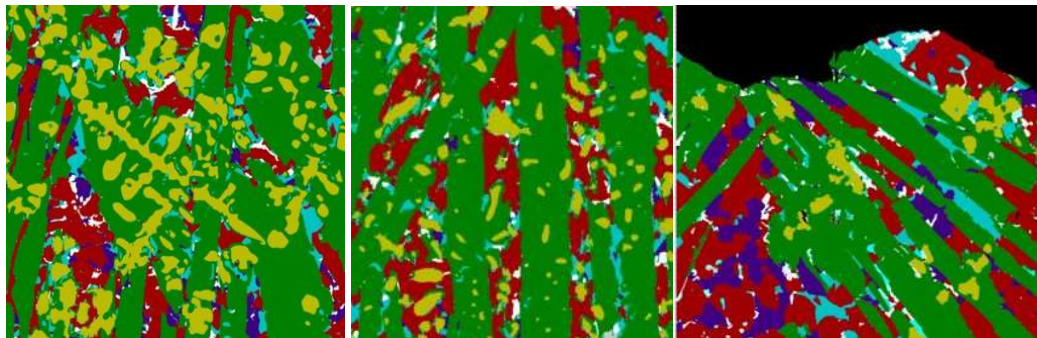


*Figure 4. Main features observed in the microstructure taken from other samples (Composition very close to Alloy 1 but produced in the plant)*

### 3.2. Thermodynamic modelling results

Since the experimental samples have solidified under normal casting conditions, it is expected that the resulting phase fractions lie somewhere between the limiting cases of equilibrium and the Scheil approximations. Equilibrium solidification assumes infinite diffusivity of elements in the solid region, whereas Scheil solidification assumes zero diffusion in the solid region. Infinite diffusivity in the liquid region is assumed in both cases. Comparisons of the predicted phase fractions of these two limiting cases with experimental phase fractions quantified with AMICS are shown in Figure 5.

As expected, neither of the two provides an accurate estimate. Under equilibrium conditions, the amount of $FeSi_2$ is overestimated. Furthermore, a small fraction of pure Si phase, which is found experimentally for both samples (Alloy 1 and Alloy 2), is not present in equilibrium solidification simulations. On the other hand, in the Scheil approximation, too much of the FeSi phase is present at the end of the solidification. Additionally, only a very small fraction of the low-temperature $\beta$-$FeSi_2$ phase is formed at the end of solidification as no transformation of the high temperature $\alpha$-$FeSi_2$ phase

(present in the thermodynamic database as $Fe_3Si_7$) could occur (it would require diffusion in the solid phase because of the different stoichiometry).

Simulated evolution of the phase fractions with decreasing temperature under equilibrium and Scheil conditions are shown in Figure 5 (b-c) for Alloy 1 and Figure 5 (e-f) for Alloy 2. The FeSi phase forms first at approximately 1500 K. At ~1400 K, the high-temperature $Fe_3Si_7$ phase starts to form. Under equilibrium conditions, the formation of $Fe_3Si_7$ consumes some of the FeSi during formation, in a peritectic reaction with the liquid. At 1250 K, the low temperature $FeSi_2$ phase forms, which fully transforms $Fe_3Si_7$ into its low temperature form by partly consuming FeSi. Finally, at 1220K the $Mg_2Si$ phase forms and the system reaches full solidification (neglecting the other elements). Within the Scheil approximation on the other hand, no solid-solid transformation can take place. This prevents solid transformation of FeSi as seen during equilibrium solidification, which increases the Si concentration in the liquid, resulting in the formation of a fraction of pure Si phase at the end of the solidification, however, overestimated compared to experimental values.
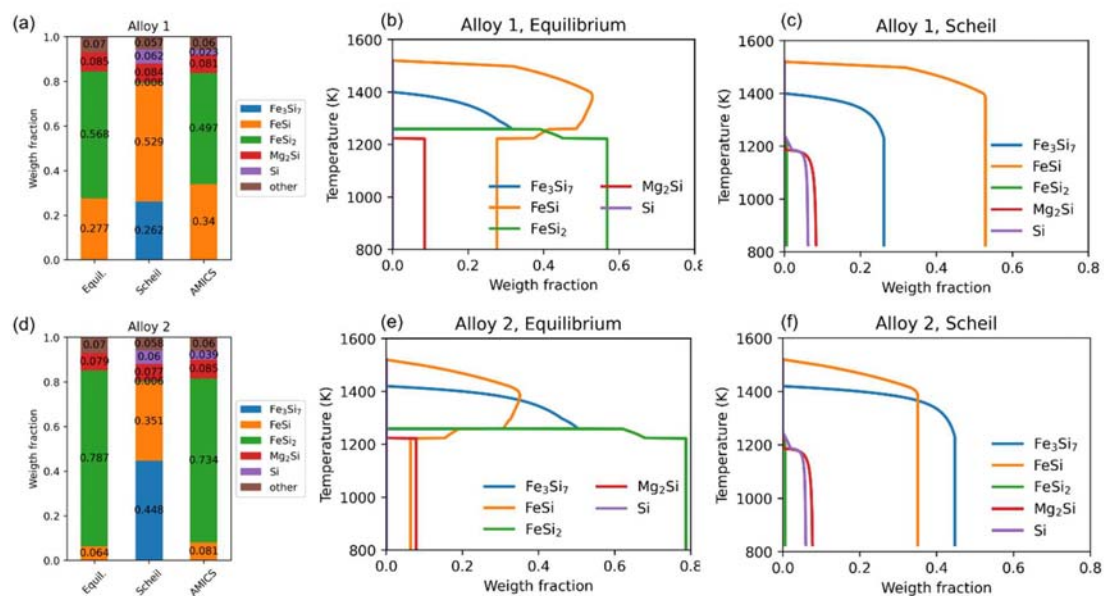


*Figure 5 Phase fractions of main phases formed in Alloy 1 and Alloy 2 during solidification. (a/d) Comparison of resulting phase fractions at end of solidification between simulations under Equilibrium and Scheil approximations, and experimental phase fractions from AMICS. (b/e) Evolution of phases in Alloy 1/Alloy 2 with decreasing temperature under equilibrium conditions. (c/f) Evolution of phases in Alloy 1/Alloy 2 with decreasing temperature under Scheil conditions.*

To fit the experimental measurements more accurately, a model intermediate to Scheil and Equilibrium is needed. Experimental observations shown in Figure 4 suggest the transformation of FeSi to $FeSi_2$. Indeed, part of the FeSi2 phase is not present as big rods but has the same morphology and seems to replace the FeSi phase. Thus, we need to include solid-solid reactions to obtain an improved model for the FSM alloys. Initially, one solid-solid reaction was implemented yielding $FeSi_2$ as a product, according to:

$$Fe_3Si_7 + FeSi \rightarrow 4\ FeSi_2 \qquad\qquad (Reaction\ 1)$$

This reaction aligns with the equilibrium solidification simulation at ~1250 K, where $Fe_3Si_7$ is fully consumed to produce $FeSi_2$. As accurate experimental data for the thermal history of the alloys was not available, a constant cooling rate of 2 K/s was assumed in the model calibration. This assumption does not affect the methodology and trends presented in the following paragraphs, only the calibration of the model parameters. As an initial approach the model was calibrated with Alloy 1, by varying the

reaction rate constant $K(T)$ of Reaction 1, which enters the JMAK equation (Equation 1). The resulting phase fractions were compared with AMICS data of Alloy 1. The rate constant is dependent on the frequency factor $K0$ and the activation energy $Qr$. To simplify calibration and in the absence of multiple cooling rates, $Qr$ was fixed and $K_0$ was varied from $10^{-9}$ to $10^{-7}$ as seen in Figure 6(a). A larger value of $K_0$ corresponds to a higher reaction rate.
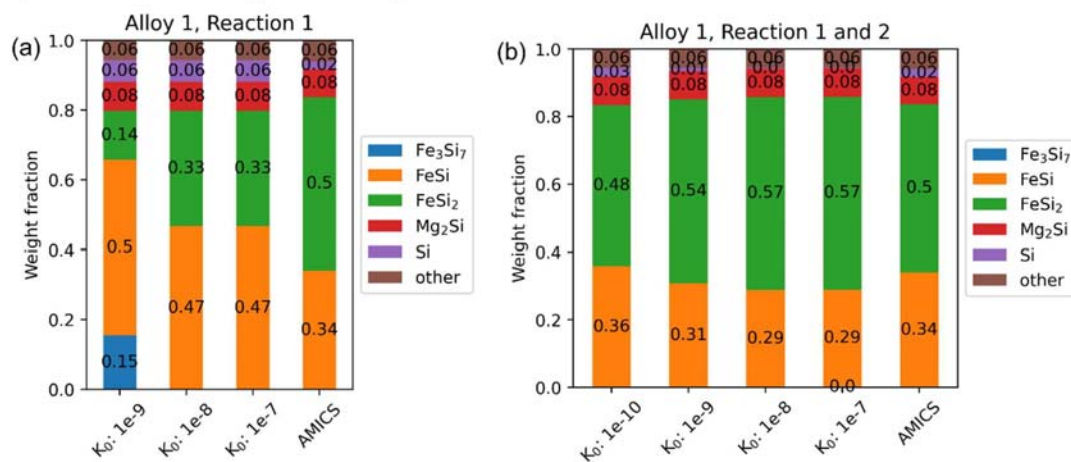


*Figure 6 Comparison of calculated phase fractions in Alloy 1, by variation of the frequency factor K0 with experimental phase fractions from AMICS (a) when including Reaction 1, (b) when including both Reaction 1 and Reaction 2.*

The experimental phase fractions from AMICS are shown to the right in Figure 6(a). A $K_0$ value of $10^{-9}$ results in a too low reaction rate to consume all the high temperature $Fe_3Si_7$. By increasing the $K_0$ value to $10^{-8}$, this results in full consumption of the $Fe_3Si_7$ phase. However, continuing to increase $K_0$ beyond this value has no effect, since all $Fe_3Si_7$ is consumed. It is evident that this reaction alone does not accurately predict the experimental phase fractions, suggesting that additional reactions should be included. Including only Reaction 1, the amount of Si is overestimated whereas the amount of $FeSi_2$ is underestimated. A second reaction was therefore included in the model, according to:

$$FeSi + Si \rightarrow FeSi_2 \quad\quad\quad\quad (Reaction\ 2)$$

Where FeSi and Si are consumed to yield $FeSi_2$. Figure 4(b) shows the resulting phase fractions when varying $K_0$ for Reaction 2 between $10^{-10}$ and $10^{-7}$. When including this second reaction, a very good agreement with experimental phase fractions is achieved with $K_0=10^{-10}$, for all main phases.

Even though including both Reaction 1 and Reaction 2 in the model gives a very good correspondence with the experimental data, it is seen from the temperature evolution of phases in the equilibrium simulation, that also a peritectic reaction with FeSi and Si from the liquid to form $Fe_3Si_7$ at high temperature takes place:

$$3\ FeSi + Si\ (L) \rightarrow Fe_3Si_7 \quad\quad\quad\quad (Reaction\ 3)$$

This would result in formation of more Fe3Si7 at high temperature, than is predicted in the current model, which also would result in more formation of FeSi2 by Reaction 1 and also less pure Si later on in the solidification. Thus, even though including Reaction 2 in our model gives very good agreement with experiment, it may not reflect the actual reactions taking place, simply that Reaction 2 results in the same phase fractions at the end of solidification as Reaction 3 combined with Reaction 1. It is also possible that both Reaction 2 and Reaction 3 take place to some extent. In the absence of additional experimental results like interrupting solidification with quenching, it is not possible to conclude on the prevalence of these reactions.

Nevertheless, the phase fractions at end of solidification are well captured for Alloy 1. The optimized rate constants for Reaction 1 and Reaction 2 for Alloy 1 were applied to Alloy 2, to test the

validity or robustness of these parameters across different alloys. Figure 7 shows the resulting simulated phase fractions of Alloy 1 (left) and Alloy 2 (right), compared with AMICS. While the amount of Si is slightly underestimated and FeSi overestimated in the simulation, there is a very good agreement between model and experiment.
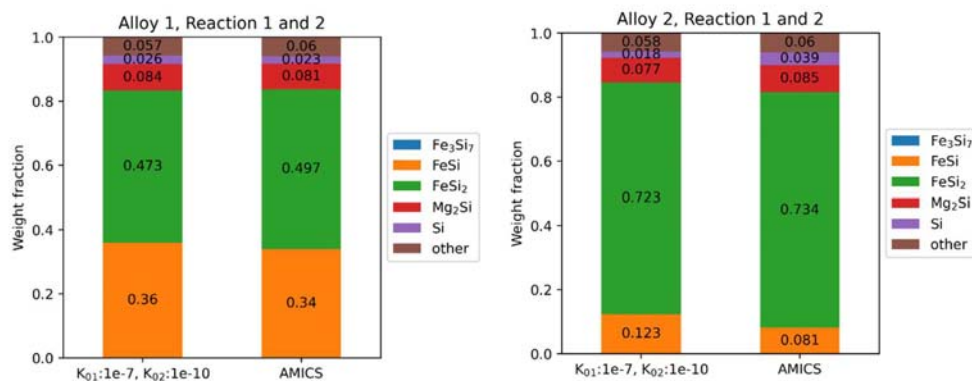


*Figure 7 Comparison of modelled phase fractions and experimental phase fractions from AMICS in Alloy 1 (left) and Alloy 2 (right) with calibrated JMAK parameters for Reaction 1 and Reaction 2.*

### 3.3. Phase field modelling results

Parts of the solidification process were further investigated by phase field modelling using Micress software [3]. To this end, extensive calibration of numerical parameters was needed as it is often difficult to relate parameters with the physical properties of the phases. The phase field model was first calibrated to reproduce the dendritic morphology of the FeSi phase upon initial nucleation and growth, by tuning the diffusion parameters in the liquid, and the properties of the FeSi/liquid interface: surface energy and kinetic coefficients. Parameters were first tuned to reproduce the FeSi morphology of Alloy 2 and further applied to Alloy 1 to check the validity of the parameter set across different alloys. The simulation domain boundary conditions are periodic in phase and composition, and uniform temperature with an imposed, constant cooling rate or heat flux. The resulting morphologies of the formed FeSi dendrites at 1450K upon parameter calibration for alloys 1 and 2 are shown in Figure 8. The same set of parameters can correctly produce the more dendritic morphology of the FeSi phase observed in experimental samples of Alloy 2 while also yielding the rounder FeSi morphology as seen in experimental samples of Alloy 1. The seed density has been adjusted to be realistic but not really calibrated to replicate the experimental results.



*Figure 8 Nucleation and initial growth of FeSi (white) in liquid (red) at 1450K for Alloy 1 (left) and Alloy 2 (right)*

Following the calibration of FeSi phase formation, the phase field model was modified to include the formation of $Fe_3Si_7$. The $FeSi_2$ phase is observed experimentally to have a more elongated, rod-like, phase morphology due to its crystalline structure. It is assumed that the high temperature form is also similar. This was obtained by setting tetragonal anisotropy parameters within the model.

Upon establishing a phase field model with parameters that correctly reproduced the morphology of the FeSi and $Fe_3Si_7$ phase, the nucleation and growth of $Fe_3Si_7$ in the presence of FeSi was investigated. Simulations were run from an initial configuration where some FeSi grains were present in the liquid (Figure 9(left)). As seen in Figure 9 (middle) $Fe_3Si_7$ (white phase) preferentially nucleates in the close vicinity of an FeSi grain (orange phase). This can be reasoned by the change in the local liquid concentration where the FeSi phase first nucleates and grows. Locally, the formation of FeSi results in a surplus of Si in the liquid close to FeSi grains, which creates a driving force for nucleation of $Fe_3Si_7$, as the Si concentration in this phase is higher than the average in the liquid. This nucleation mode was activated by defining the FeSi/Liquid interface as a nucleation site in addition to the random seed distribution.
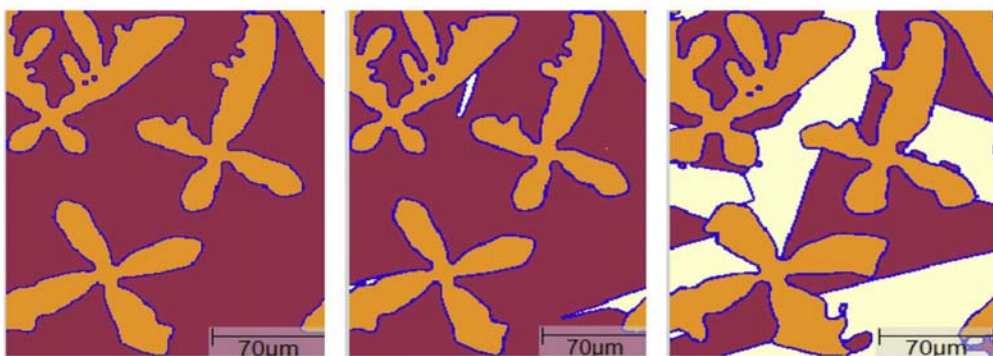


*Figure 9 Initial structure of FeSi (orange), nucleation of FeSi₂ (white) on top of said structure, growth of FeSi₂*

As seen from the equilibrium solidification path for the two alloys (Figure 5), the FeSi phase and the $Fe_3Si_7$ phase both grows simultaneously down to around 1380K. Below this temperature, the amount of $Fe_3Si_7$ continues to increase whereas FeSi decreases, suggesting some degree of competitive growth between the two phases. The phase interaction between FeSi and $Fe_3Si_7$ below 1380K was further investigated by the phase field model to explore the effect of morphology on this interaction. Three simulations were set up to study FeSi, $Fe_3Si_7$ and liquid interactions with three different initial idealized morphologies, as shown in Figure 10(left panel). In the first case (upper left), 85% of the FeSi surface is covered by $Fe_3Si_7$. The remaining 15% area of FeSi is in contact with the liquid. In the second case (middle left) 45% of the FeSi surface is covered with $Fe_3Si_7$, whereas 55% is in contact with the liquid. In the latter case (lower left) 100% of the FeSi surface is in contact with the liquid, such that there is no contact between the FeSi and the $Fe_3Si_7$ phase. In all three simulations, the FeSi phase has initial contact with the liquid. Simulations were initialized with a temperature of 1360 K and a constant cooling rate was applied. No new nucleation was allowed. The evolution of the FeSi and $Fe_3Si_7$ from the three different initial morphologies is seen in Figure 10 (right panel).

Table 2 lists the resulting phase fractions of FeSi and $Fe_3Si_7$ with the three levels of coverage of the FeSi phase. The differences indicate that the positioning of the phases relative to each other has a significant influence on the rest of the solidification process. In the two upper configurations, where FeSi is in contact with $Fe_3Si_7$ and the liquid, the $Fe_3Si_7$ phase grows by reaction with FeSi and the liquid, resulting in a partial consumption of the FeSi phase as well as formation of an envelope of $Fe_3Si_7$ around the FeSi phase, thus sealing it away from the liquid. This is also observed in the AMICS maps where every FeSi grain, even those far from the bulk of the FeSi₂, is covered by a thin layer of FeSi₂. At this point further growth of the FeSi phase is largely hindered. This is because the solid-solid phase boundaries are much less mobile than the solid-liquid phase boundaries. Thus, when FeSi is no longer in direct contact with the liquid, further growth would rely on solid state diffusion which is orders of magnitude smaller than liquid diffusion of elements. In the latter case, the FeSi phase has continued access to the liquid throughout the whole solidification interval considered. This simple case study illustrates the importance of nucleation and growth sequence on the final microstructure.
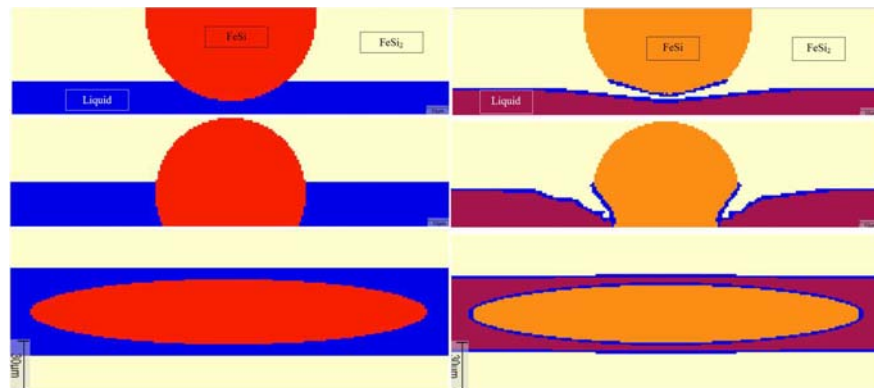
*Figure 10. Simulations at 1360K (left) and 1250 K (right). Top to bottom: 85%Coverage simulation, 45%Coverage simulation, 0%Coverage simulation. The phase noted Fe$_3$Si$_7$ corresponds to high temperature phase Fe$_3$Si$_7$.*

*Table 2 Resulting phase fractions of FeSi and Fe$_3$Si$_7$ with the three levels of coverage of the FeSi phase.*

|                | FeSi mass fraction | Fe$_3$Si$_7$ mass fraction |
|----------------|--------------------|----------------------------|
| **0% Coverage**    | 0.238          | 0.661                      |
| **45%Coverage**    | 0.301          | 0.560                      |
| **85%Coverage**    | 0.304          | 0.552                      |

## 4. Concluding remarks

Thermodynamic modelling and phase field modelling was applied to the solidification of FSM alloys. The thermodynamic database developed at SINTEF covers well the range of composition encountered in commercial alloys. Dedicated experiments were carried out and the microstructure characterized on large areas to get proper statistics of phase fractions using the AMICS. The results showed the necessity to consider solid-solid transformation to accurately predict the phase distribution. The phase field model has enabled us to study the effect of phase morphology and spatial distribution during the solidification process and the consequences on the final phase fractions.

This work is only a first step and additional key elements should be included with the phase they are forming. Inclusion of rate earth elements is particularly important, but it requires an extension of the thermodynamic database and addition of phases not properly documented.

### Declaration of competing interest

The authors declare that they have no known competing financial interests or personal relationships that could have appeared to influence the work reported in this article.

### Acknowledgments

### References

[1]   Hartung C., White D., Copi K. et al. The Continuing Evolution of MgFeSi Treatments for Ductile and CG Irons. Inter Metalcast 8, 7–15 (2014). https://doi.org/10.1007/BF03355577
[2]   ThermoCalc, https://thermocalc.com/
[3]   Micress, https://micress.rwth-aachen.de/
[4]   AMICS, https://www.bruker.com/en/products-and-solutions/elemental-analyzers/eds-wds-ebsd-SEM-Micro-XRF/software-amics-automated-mineralogy-system.html